

1 **Induction of viral mimicry upon loss of DHX9 and ADAR1 in breast cancer cells**

2 Kyle A. Cottrell ^{1,4,5†*}, Sua Ryu ^{1,4‡}, Luisangely Soto Torres ^{1,4}, Angela M. Schab ^{1,4}, Jason D.
3 Weber ^{1,2,3,4*}

4 ¹Department of Medicine, Division of Molecular Oncology, ²Department of Cell Biology and
5 Physiology, and ³Department of Biology, Siteman Cancer Center, ⁴ICCE Institute, Washington
6 University School of Medicine, Saint Louis, Missouri, USA

7 ⁵Department of Biochemistry, Purdue University, West Lafayette, IN, USA

8 ‡ Authors contributed equally

9 *Co-Corresponding authors

10

11 Correspondence:

12 Kyle A Cottrell, Ph.D.
13 Department of Biochemistry
14 Purdue University
15 201 S University St.
16 West Lafayette, IN
17 Email: cottrellka@pudue.edu
18 Telephone: 765-494-6941

19

20 Jason D. Weber, Ph.D.
21 Department of Medicine
22 Division of Molecular Oncology
23 Washington University School of Medicine
24 660 South Euclid Avenue
25 Campus Box 8069
26 St. Louis, MO 63110 USA
27 Email: jweber@wustl.edu
28 Telephone: 314-747-3896
29 Fax: 314-362-0152

30

31 **Abstract**

32 Detection of viral double-stranded RNA (dsRNA) is an important component of innate immunity.
33 However, many endogenous RNAs containing double-stranded regions can be misrecognized
34 and activate innate immunity. The interferon inducible ADAR1-p150 suppresses dsRNA
35 sensing, an essential function for ADAR1 in many cancers, including breast. Although ADAR1-
36 p150 has been well established in this role, the functions of the constitutively expressed
37 ADAR1-p110 isoform are less understood. We used proximity labeling to identify putative
38 ADAR1-p110 interacting proteins in breast cancer cell lines. Of the proteins identified, the RNA
39 helicase DHX9 was of particular interest. Knockdown of DHX9 in ADAR1-dependent cell lines
40 caused cell death and activation of the dsRNA sensor PKR. In ADAR1-independent cell lines,
41 combined knockdown of DHX9 and ADAR1, but neither alone, caused activation of multiple
42 dsRNA sensing pathways leading to a viral mimicry phenotype. Together, these results reveal
43 an important role for DHX9 in suppressing dsRNA sensing by multiple pathways.

44

45

46

47

48

49

50

51

52

53 **Introduction**

54 RNA editing enhances protein diversity and modulates multiple aspects of RNA
55 metabolism¹⁻³. A-to-I editing is carried out by adenosine deaminase acting on RNA 1 (ADAR1),
56 an RNA editase that binds double-stranded RNA (dsRNA) and converts adenosines to
57 inosines^{4,5}. The main domains of ADAR1 include the Z-DNA binding domains (ZBD), the
58 double-stranded RNA (dsRNA) binding domains (dsRBD), and the deaminase domain^{6,7}. There
59 are two isoforms, p110 and p150, produced by alternative transcriptional start sites⁸. They share
60 the same deaminase domain, dsRBDs, and a ZBD, but exhibit a distinct subcellular
61 localization^{9,10}. ADAR1-p150 is predominantly cytoplasmic, whereas ADAR1-p110 is nuclear-
62 localized^{9,11}.

63 An important role for ADAR1 is to suppress dsRNA sensing¹²⁻¹⁵. Many endogenously
64 encoded RNAs can form large double-stranded regions, often through base-pairing between
65 inverted Alu elements¹⁶. ADAR1 edits the majority of human genes, with most editing occurring
66 within inverted Alu repeats^{3,4}. By binding, editing, and thus altering the structure of dsRNA,
67 ADAR1 suppresses the detection of dsRNA by various cytoplasmic sensors such as MDA5,
68 RIG-I, and PKR^{12,13,15,17}. These RNA sensors are part of innate immunity against viral
69 infections^{16,18-20}. Thus, ADAR1 prevents the activation of innate immunity pathways by
70 endogenous immunogenic RNAs^{16,19,21}.

71 The cell-intrinsic antiviral response against foreign dsRNA - or misrecognized
72 endogenous dsRNA - involves multiple pathways: (1) Recognition of dsRNA by MDA5 or RIG-I
73 results in the activation of type I interferon (IFN-I) signaling^{16,19,21}. (2) Activation of the dsRNA-
74 binding kinase PKR triggers translational shutdown by phosphorylation of the translation
75 initiation factor eIF2a¹². (3) Detection of dsRNA by OAS proteins activates RNase L, which
76 carries out non-specific cleavage of RNA and triggers cell death²². There is significant crosstalk
77 between the three pathways, and the aforementioned dsRNA sensors are transcriptionally

78 controlled by IFN-I, known as interferon-stimulated genes (ISGs)^{23,24}. The ADAR1-p150 isoform
79 is itself an ISG and is the isoform responsible for suppressing the activation of dsRNA
80 sensors^{8,10,14,25}. ADAR1-p110, however, is constitutively expressed, though its functions are less
81 established^{26,27}.

82 Because IFN-I signaling is often cytotoxic and antiproliferative, ADAR1's ability to
83 suppress IFN-I signaling was shown to exert pro-tumor effects^{21,28,29}. As such, ADAR1 has been
84 proposed as a potential therapeutic target for various cancers, including breast cancer^{28,30–32}.
85 ADAR1 mRNA expression is elevated in breast cancer and is correlated with a poor
86 prognosis^{28,33}. Furthermore, ADAR1 is essential for a subset of breast cancer cells
87 overrepresented by triple-negative breast cancer (TNBC)³³. Known as 'ADAR1-dependency,'
88 depletion of ADAR1-p150 leads to IFN-I signaling and global translational repression in cells
89 that are sensitive to depletion of ADAR1^{32,33}. What makes cancer cells sensitive or refractory to
90 ADAR1 loss is not yet determined³³.

91 ADAR1 interacts with numerous RNA binding proteins including RNA helicases,
92 transcription machinery, and DNA repair proteins^{27,34–37}. The influence of ADAR1-interacting
93 proteins on A-to-I editing has previously been reported^{35,38–41}. In this study, we evaluated
94 components of the ADAR1 interactome in breast cancer cells and identified the RNA helicase
95 DHX9 as a redundant suppressor of immunogenic dsRNA in ADAR1-independent breast cancer
96 cells. We demonstrate that co-depletion of ADAR1 and DHX9 is sufficient to trigger a viral
97 mimicry phenotype in ADAR1-independent cells.

98 **Results**

99 **Proximity Labeling by APEX2 Reveals ADAR1 Interacting Proteins**

100 To better understand the role of ADAR1-p110 in breast cancer, we turned to a proximity
101 labeling approach using APEX2 to identify putative ADAR1-p110-interacting proteins. Proximity
102 labeling by APEX2 allows for the identification of proteins within 20 nm of an APEX2 fusion
103 protein via biotin-mediated pulldown⁴². An APEX2-ADAR1-p110 fusion construct or APEX2
104 alone was expressed in MDA-MB-231, MCF-7, and SK-BR-3 (Fig. 1a). Following proximity
105 labeling, biotinylated proteins were purified by streptavidin pulldown and subsequently identified
106 by mass spectrometry (Fig 1b-c, Extended Data Fig. 1a, Supplementary Table 2). In total, we
107 identified over one hundred enriched proteins across the three cell lines, with many identified in
108 all three lines (Fig. 1d). Over-representation analysis of gene ontology (GO) terms revealed that
109 many of the proteins identified by proximity labeling have roles in multiple aspects of RNA
110 metabolism and localize to the nucleus and nucleolus (Fig. 1e, Supplementary Table 3). This
111 finding was supported by a comparison to proteins previously observed to localize to the
112 nucleus and nucleolus within MCF-7 in the SubCellBarcode dataset⁴³ (Fig.1f and 1g). These
113 findings are largely consistent with the localization of ADAR1 within the cell lines studied.
114 Immunofluorescence for ADAR1, which largely reflects the localization of ADAR1-p110 as the
115 predominant isoform, showed that ADAR1 was localized in both the nucleus and nucleolus (Fig.
116 1h).

117 **Validation of Protein Interactions Identified by Proximity Labeling**

118 Although proximity labeling by APEX2 is a powerful technique for identifying putative
119 protein-protein interactions, it does not distinguish between interactions and close
120 associations⁴². To validate the proximity labeling findings and provide supporting evidence for
121 direct protein-protein interactions, we performed co-immunoprecipitation followed by
122 immunoblotting for five proteins identified by proximity labeling. ADAR1 could be
123 immunoprecipitated by antibodies against the helicases DHX9, DDX17, and DDX54 (Fig. 2a-g).
124 ADAR1 could also be immunoprecipitated with antibodies against XRN2 and PARP (Extended

125 Data Fig. 1b-c). To assess whether these potential interactions depended on RNA, we treated
126 the lysates with RNase A to degrade RNA prior to immunoprecipitation (Extended Data Fig. 1d).
127 Immunoprecipitation of ADAR1 by antibodies against DHX9, DDX17, and DDX54 was possible
128 even in the presence of RNase A and improved in some cases (Fig. 2a-g). For DDX17 and
129 DDX54, RNase A treatment did not change the co-immunoprecipitation results. However, DHX9
130 immunoprecipitated with both isoforms of ADAR1 in the absence of RNase A, but only with
131 ADAR1-p110 when treated with RNase A. These findings suggest that DHX9, DDX17, and
132 DDX54 directly interact with ADAR1-p110, and DHX9 interacts with ADAR1-p150 through an
133 RNA bridge/scaffold. The co-immunoprecipitation findings are also consistent with the
134 localization of the proteins studied. Much like ADAR1, the helicases DHX9, DDX17, and DDX54
135 localized to the nucleus or nucleolus (Fig. 2h-j). Together, these findings validate the results of
136 the proximity labeling described in Fig. 1 and provide evidence for direct interactions between
137 ADAR1 and multiple helicases.

138 **DHX9 is overexpressed in breast cancer**

139 Of the identified helicases, DHX9 was of particular interest for several reasons. First,
140 DHX9 is the only helicase in humans that has a dsRBD. The dsRBD that is present in DHX9 is
141 of the same class present in ADAR1 and PKR (Fig. 3a). Analysis of publicly available RNA-seq
142 data for human cell lines and tumors revealed that DHX9 expression closely correlates with
143 ADAR1 expression (Fig. 3b-d, Extended Data Fig. 2a-c). The correlation is stronger between
144 DHX9 and the transcript encoding ADAR1-p110, than between DHX9 and ADAR1-p150 (Fig.
145 3c-d, Extended Data Fig. 2d-e). Furthermore, the expression of DHX9 and ADAR1 correlates
146 better than any other helicase identified by proximity labeling (Fig. 3b, Extended Data Fig. 2b).
147 Consistent with this correlated expression, and much like ADAR1, DHX9 is highly expressed in
148 breast cancer and is correlated with a poor prognosis³³ (Fig. 3c, Extended Data Fig. 2f-h).

149 **DHX9 is essential in TNBC cell lines and suppresses PKR activation**

150 The similarities between ADAR1 and DHX9 led us to further study the role of DHX9 in
151 breast cancer. Analysis of publicly available data from DepMap
152 (<https://depmap.org/portal/download/custom/>) revealed that DHX9 is commonly essential in
153 breast cancer cell lines (Fig. 3f). We validated this finding by knocking down DHX9 in four TNBC
154 cell lines previously shown to be ADAR1-dependent³³. In all four lines, knockdown of DHX9
155 caused cell death, likely through caspase-mediated apoptosis as indicated by cleaved PARP
156 (Fig. 3g and h). Given the presence of the common dsRBD in DHX9 and PKR, and the role of
157 DHX9 in regulating the abundance of dsRNA⁴⁴, we asked whether DHX9 could influence
158 activation of PKR. To our surprise, we found that in three of the TNBC cell lines studied,
159 knockdown of DHX9 caused activation of PKR (Fig. 3g and 3i). Together these findings show
160 that DHX9 is essential in breast cancer cell lines and that in some ADAR1-dependent cell lines,
161 DHX9 suppresses PKR activation.

162 **DHX9 and ADAR1 redundantly suppress PKR activation**

163 The experiments above were performed in ADAR1-dependent TNBC cell lines - cell
164 lines that activate PKR following ADAR1 knockdown³³. We were curious if DHX9 knockdown
165 would also cause PKR activation in ADAR1-independent cell lines - cell lines that do not
166 activate PKR following ADAR1 knockdown. Using shRNAs, we knocked down DHX9 in two
167 ADAR1-independent breast cancer lines, MCF-7 and SK-BR-3 (Fig. 4a-b and 4f-g, Extended
168 Data Fig. 4a-b and 4g-h). Unlike in ADAR1-dependent cell lines, knockdown of DHX9 did not
169 cause activation of PKR in ADAR1-independent cell lines (Fig. 4a, 4d, 4f, 4i). Next, we asked
170 whether combined knockdown of ADAR1 and DHX9 in these cell lines would lead to activation
171 of PKR. As we had previously observed, knockdown of ADAR1 in SK-BR-3 and MCF-7 did not
172 cause PKR activation³³. However, combined knockdown of DHX9 and ADAR1 caused robust

173 activation of PKR in both cell lines (Fig. 4a, 4d, 4f, 4i). Consistent with PKR activation, we
174 observed increased phosphorylation of the PKR substrate eIF2 α following combined knockdown
175 of ADAR1 and DHX9 (Fig. 4a and 4d, Extended Data Fig. 4c and 4i). Like in ADAR1-dependent
176 TNBC cell lines, knockdown of DHX9 caused reduced proliferation of MCF-7 and SK-BR-3 (Fig.
177 4c, 4d, 4h, 4j), likely through caspase-dependent apoptosis, as indicated by elevated cleaved
178 PARP (Fig. 4a, 4d, Extended Data Fig. 4e, 4k). Although PARP cleavage was increased upon
179 combined knockdown of DHX9 and ADAR1, this did not statistically reduce the proliferation of
180 the cells compared to single knockdown of ADAR1 and DHX9 as measured by foci formation.
181 Together, these results reveal that ADAR1 and DHX9 redundantly suppress PKR activation in
182 ADAR1-independent breast cancer cell lines.

183 **DHX9 and ADAR1 redundantly suppress RNase L activation**

184 Next, we wanted to evaluate the activation of other dsRNA sensing pathways in ADAR1-
185 independent cell lines after the combined knockdown of ADAR1 and DHX9. To assess whether
186 the IFN-I pathway, or other pathways, is activated after combined knockdown of ADAR1 and
187 DHX9 we turned to analysis of differential gene expression by RNA-seq. In the process of
188 preparing RNA for sequencing, we were surprised to find specific degradation of rRNA in MCF-7
189 cells following combined knockdown of ADAR1 and DHX9 (Fig. 4k). Single knockdown of either
190 DHX9 or ADAR1 did not cause rRNA degradation. The observed rRNA degradation in the
191 combined knockdown cells was reminiscent of the degradation products caused by RNase L⁴⁵.
192 Transfection with poly(I:C), which activates the IFN-I pathway and RNase L⁴⁶, created an
193 identical band pattern to that of combined knockdown of DHX9 and ADAR1, indicating that the
194 degradation of rRNA observed in these cells is likely caused by RNase L activity (Fig. 4k). We
195 performed the same experiment with the ADAR1-dependent TNBC cell lines described above.
196 In these cells, we did not see activation of RNase L after the knockdown of DHX9 alone
197 (Extended Data 3h).

198 **DHX9 and ADAR1 redundantly suppress multiple innate immunity pathways**

199 RNA sequencing revealed that many more RNAs were differentially expressed after
200 combined knockdown of DHX9 and ADAR1, compared to single knockdown of ADAR1 or DHX9
201 (Fig. 5a, Extended Data Fig. 5a-f). Analysis of differential gene expression by gene set
202 enrichment after combined knockdown of ADAR1 and DHX9 in MCF-7 revealed activation of
203 multiple pathways involved in the innate response to viral infection and repression of several
204 pathways involved in translation (Fig. 5b and Supplemental Table 14). An enrichment map
205 showed that the activated pathways associated with innate immunity formed one cluster and the
206 depressed pathways formed a separate cluster (Extended Data Fig. 5g). Of the upregulated
207 pathways, several were associated with activation of IFN signaling (Fig. 5b, and Supplementary
208 Table 14). Analysis of core ISG expression revealed significant upregulation of ISGs in MCF-7
209 after combined knockdown of ADAR1 and DHX9 (Fig. 5c and Extended Data 5c). On the
210 contrary, knockdown of DHX9 or ADAR1 alone did not increase ISG expression. Activation of
211 RNase L described above also indicated that the type I IFN pathway was active in MCF-7 after
212 double knockdown of DHX9 and ADAR1, because the activators of RNase L, the OAS proteins,
213 are ISGs²². In fact, a GO term associated with OAS activity was upregulated in MCF-7 after
214 combined knockdown of ADAR1 and DHX9 (Supplementary Table 14). Consistent with
215 activation of PKR, we also observed increased expression of ATF4 targets (Fig. 5d) and NF- κ B
216 targets (Fig. 5e). Interestingly, we did not observe activation of any of these pathways or RNase
217 L in SK-BR-3 following combined ADAR1 and DHX9 knockdown.

218 The finding that combined knockdown of ADAR1 and DHX9 did not induce ISG
219 expression in SK-BR-3 is consistent with our findings in TNBC cell lines. While knockdown of
220 DHX9 alone caused activation of PKR in several TNBC cell lines, we observed no activation of
221 the type I IFN pathway, as indicated by no change in ISG15 expression (Extended Data Fig. 3f-
222 g). ISG15 was found to be highly upregulated at the RNA and protein level in MCF-7 after

223 double knockdown of ADAR1 and DHX9 (Extended Data Fig. 4f, 4m, Supplementary Table 8).
224 Like ISG expression overall, ISG15 expression in SK-BR-3 was not changed by knockdown of
225 DHX9 and/or ADAR1 (Extended Data Fig. 4l, 4n).

226 Given the previously described role of DHX9 in the control of Alu containing RNAs, we
227 next sought to assess if increased expression of transposable elements, especially Alus, could
228 explain the activation of PKR or the IFN pathway upon combined knockdown of DHX9 and
229 ADAR1. Analysis of our RNA-seq data revealed that transposable element expression was
230 generally unchanged upon either single knockdown of ADAR1 or DHX9, or combined
231 knockdown of both proteins (Extended Data Fig. 6a-f).

232 **The dsRBDs of DHX9 are sufficient to suppress PKR activation in the absence of ADAR1**

233 Having shown through knockdown studies that ADAR1 and DHX9 function redundantly
234 to suppress dsRNA sensing, we next wanted to assess which functions of DHX9 and which
235 isoforms of ADAR1 are important for this role. To determine which functions of DHX9 are
236 sufficient to suppress PKR activation, we performed a rescue experiment with wild-type DHX9,
237 a helicase deficient mutant DHX9, and a truncated DHX9 that possess the N-terminal dsRBDs
238 fused to EGFP (Fig. 6a). Overexpression of wild-type DHX9 rescued the PKR activation
239 phenotype caused by double knockdown of ADAR1 and DHX9, confirming that the observed
240 phenotypes are not an off-target effect of the shRNAs used for knockdown (Fig. 6b and 6d).
241 Interestingly, the DHX9^{K417R} mutant, which lacks helicase activity due to its inability to bind
242 ATP⁴⁷, was also capable of suppressing PKR activation. The same was true for a construct
243 which contained the dsRBDs of DHX9 fused to EGFP (dsRBD-EGFP). These findings indicate
244 that the DHX9 dsRBDs are likely sufficient to suppress PKR activation in the absence of ADAR1
245 and DHX9. However, only wild-type DHX9 could rescue the reduced foci formation observed

246 after DHX9 knockdown (Fig. 6c and 6e). This finding indicates that the PKR activation
247 phenotype and the reduced proliferation phenotype are uncoupled.

248 Consistent with the observation that the DHX9 dsRBDs are sufficient to suppress PKR
249 activation, knockdown of DDX17, which lacks dsRBDs, did not cause substantial PKR activation
250 in SK-BR-3 (Extended Data Fig. 9). Unlike DHX9, knockdown of DDX17 had no effect on cell
251 proliferation as measured by the foci formation assay (Extended Data Fig. 9b and 9d). While
252 combined knockdown of DHX9 and ADAR1 in SK-BR-3 caused a 5-10 fold increase in PKR
253 phosphorylation, the combined knockdown of DDX17 and ADAR1 caused only a modest 1.5-
254 fold increase in PKR phosphorylation (Extended Data Fig. 9a and 9c). This finding underscores
255 the novel role of the DHX9 helicase and its dsRBD, a unique domain among this large family of
256 RNA helicases.

257 **The p110 and p150 isoforms of ADAR1 suppress PKR activation in the absence of DHX9**

258 Next, we turned to ADAR1, and asked which isoform of ADAR1 is sufficient to suppress
259 PKR activation in the absence of DHX9. We used the same approach as above, a rescue
260 experiment with overexpression of ADAR1-p110 or ADAR1-p150. Interestingly, we found that
261 both ADAR1 isoforms were sufficient to suppress PKR activation upon loss of DHX9 (Fig. 6f and
262 6h, Extended Data Fig. 8a-b). However, overexpression of neither ADAR1 isoform was able to
263 rescue the foci formation phenotype, again indicating that the PKR activation and cell
264 proliferation phenotypes are uncoupled (Fig. 6g and 6i).

265 **Discussion**

266 In recent years, ADAR1 has become an important therapeutic target for breast and other
267 cancers. It is clear from the literature that depletion of ADAR1 in ADAR1-dependent cell lines
268 leads to activation of dsRNA sensors and innate immunity programs that lead to cell
269 death^{21,32,33}. Yet unclear is what distinguishes ADAR1-dependent cell lines from ADAR1-

270 independent cell lines - those that are insensitive to ADAR1 depletion. Elevated ISG expression
271 has been proposed as a potential prerequisite for ADAR1-dependency, but some ADAR1-
272 independent cell lines exhibit elevated ISG expression^{21,33}. As such, more information is needed
273 to identify the factors that establish ADAR1-dependency or ADAR1-independency. To begin to
274 fill in some of the knowledge gaps surrounding ADAR1, we utilized proximity labeling to identify
275 putative ADAR1 interacting proteins, specifically focusing on the less studied ADAR1-p110
276 isoform.

277 Of the proteins identified by proximity labeling, the DEAH box helicase DHX9 was of
278 particular interest. Like ADAR1 and PKR, DHX9 possesses dsRBDs, a singularly unique trait
279 among the DEAD/DEAH box RNA helicase family. DHX9 expression is strongly correlated with
280 ADAR1-p110 expression in breast cancer. Interestingly, both genes are located on the q-arm of
281 chromosome 1, though they are separated by 28 mb and are thus unlikely to be physically co-
282 regulated. Consistent with other reports in the literature, we show here that ADAR1 and DHX9
283 likely interact directly³⁸. We observed that ADAR1-p110 and DHX9 interact in an RNA-
284 independent manner, while the interaction between ADAR1-p150 and DHX9 was disrupted by
285 RNase treatment. This result contradicts previous findings, in which ADAR1-p150 and DHX9 co-
286 immunoprecipitated after RNase A treatment⁴⁴. This discrepancy may be due to different cell
287 lines used, HEK293T was used for the previous study, or different accessibility of DHX9
288 epitopes during immunoprecipitation. The importance of the ADAR1-DHX9 interaction is unclear
289 from this work. Further studies are needed to structurally assess the interaction and directly
290 perturb the interaction to understand what function it may have.

291 Here we report that in addition to being a commonly essential gene in breast cancer,
292 DHX9 suppresses dsRNA sensing. In ADAR1-dependent cell lines, knockdown of DHX9 alone -
293 much like knockdown of ADAR1 alone - caused activation of the dsRNA sensor PKR³³. Like
294 ADAR1 knockdown, DHX9 knockdown had no effect on PKR activation in ADAR1-independent
295 cell lines. However, combined knockdown of DHX9 and ADAR1 caused robust activation of

296 PKR in these cells. This finding indicates that ADAR1 and DHX9 function redundantly to
297 suppress PKR activation in ADAR1-independent cell lines and provides an explanation for why
298 PKR is not activated in ADAR1-independent cells upon ADAR1 knockdown. Interestingly, like
299 ADAR1, DHX9 has been shown to interact with PKR and is phosphorylated by PKR⁴⁸. More
300 research is needed to understand the importance of PKR phosphorylation of DHX9 and whether
301 or not it may serve as a feedback mechanism.

302 Rescue experiments revealed that the helicase activity of DHX9 was dispensable for
303 suppression of PKR activation. In fact, the N-terminal dsRBDs of DHX9 were sufficient to
304 suppress PKR activation in the absence of ADAR1 in ADAR1-independent cell lines. This
305 finding provides evidence for a model in which DHX9 competes with PKR for dsRNA binding
306 through its dsRBDs (Fig. 7). This competition is likely to be indirect, as DHX9 is nuclear
307 localized while PKR is generally localized in the cytosol^{49–52}. As such, DHX9 may function to
308 suppress PKR activation by sequestering dsRNAs in the nucleus.

309 Previously, the ADAR1 p150 isoform, and not the p110 isoform, was shown to be
310 responsible for suppression of PKR activation. Through rescue experiments, we show here that
311 both isoforms are sufficient to suppress PKR activation in the absence of DHX9 in ADAR1-
312 independent cell lines. A preprint that was published during the preparation of this manuscript
313 showed that the dsRBDs of ADAR1, ADAR2, and STAU1 were sufficient to suppress PKR
314 activation⁵³. Based on this finding and our rescue experiment with the DHX9 dsRBDs, it is likely
315 that ADAR1-p150 and ADAR1-p110 suppress dsRNA sensing in the absence of DHX9 by
316 competing with PKR for dsRNA binding. Although this may be direct competition in the case of
317 ADAR1-p150 localized cytoplasmically, ADAR1-p110 may function like DHX9 to sequester
318 dsRNAs in the nucleus.

319 In addition to suppression of PKR activation, we also observed that DHX9 and ADAR1
320 redundantly suppress activation of several other dsRNA sensing pathways in MCF-7.
321 Knockdown of both proteins caused activation of IFN-I signaling, likely via MDA5 activation, as

322 previously shown for ADAR1^{13,15}. We also observed activation of OAS-RNaseL and increased
323 expression of the ATF4 and NF- κ B targets, likely downstream of PKR activation^{54–56}. Taken
324 together, combined knockdown of DHX9 and ADAR1 in MCF-7 creates a viral mimicry
325 phenotype, where multiple innate immune pathways against RNA viruses have been activated
326 (Fig. 7). Interestingly, we only observed activation of PKR in other cell lines after either DHX9
327 knockdown alone or combined knockdown with ADAR1. Two possible explanations for this
328 discrepancy could be 1) Another factor may be present in some cells that suppresses dsRNA
329 sensing in the absence of DHX9 and/or ADAR1. 2) The expression of endogenous dsRNAs that
330 cause activation of sensors other than PKR may vary, leading to the differential effects of
331 ADAR1 and/or DHX9 knockdown. Further studies are needed to identify the immunogenic
332 RNAs that activate the various sensors.

333 Induction of viral mimicry has great potential as a therapeutic approach for multiple
334 cancers, including TNBC^{57–60}. In addition to the cell intrinsic effects of activating innate immune
335 pathways within the tumor, the signaling that occurs after activation of those pathways can
336 promote anti-tumor immunity, especially when combined with checkpoint inhibitors^{61–63}.
337 Combined therapies targeting ADAR1 and DHX9 may serve as an effective means of treating
338 breast and other cancers by inducing viral mimicry.

339 **Materials and Methods**

340 **Cell culture**

341 Breast cancer cell lines (MCF-7 (RRID:CVCL_0031), SK-BR-3 (RRID:CVCL_0033), BT-
342 549 (RRID: CVCL_1092), MDA-MB-231 (RRID: CVCL_0062), HCC1806 (RRID: CVCL_1258),
343 MDA-MB-468 (RRID: CVCL_0063) and 293T (RRID: CVCL_0063) were obtained from
344 American Type Culture Collection. All cell lines were cultured in Dulbecco's modified Eagle's

345 medium (DMEM) (Hyclone) with 10% fetal bovine serum (Invitrogen), 2 mM glutamine
346 (Hyclone), 0.1 mM nonessential amino acids (Hyclone), and 1 mM sodium pyruvate (Hyclone).

347 **Viral Production and Transduction**

348 Lentivirus was produced by Turbo DNAfection 3000 (Lamda Biotech) transfection of
349 293T cells with pCMV-VSV-G, pCMV- Δ R8.2, and the appropriate plasmid for expression of
350 genes of interest or shRNAs. Virus was harvested 48 hours post-transfection. Cells were
351 transduced with lentivirus for 16 hours in the presence of 10 μ g/mL protamine sulfate (Sigma-
352 Aldrich). The cells were selected with puromycin at 2 μ g/mL (Sigma-Aldrich), 150 μ g/mL
353 hygromycin (Invitrogen) or 10 μ g/mL Blasticidin (Invitrogen). The sequences for the shRNA-
354 scramble (shSCR) and shRNA-ADAR1 (shADAR1) were described and validated previously³³.
355 The sequences for shRNAs against DHX9 and DDX17 are in Supplementary Table 1.

356 **Plasmids**

357 APEX2 was PCR amplified from pcDNA3-APEX2-NES, a kind gift from the laboratory of
358 Kendall Blumer at Washington University in St. Louis. ADAR1-p110 was PCR amplified from
359 pLVX-p110-ADAR1 described previously³³. APEX2 and p110 were cloned into pLVX-IRES-puro
360 (Takara, 632183) via a series of restriction enzyme digests and ligations. The final plasmids
361 pLVX-3xFLAG-APEX2 and pLVX-3xFLAG-APEX2-linker-p110 were confirmed by digestion and
362 sequencing. The linker consists of three repeats of Gly-Gly-Gly-Gly-Ser. Lentiviral shRNA
363 constructs in the pLKO.1-puro vector were purchased as glycerol stocks from Millipore Sigma
364 (Supplemental Table 1). For shADAR1, the shRNA was subcloned into pLKO.1-hygro
365 (Addgene, #24150). Overexpression constructs for DHX9 and ADAR were generated by PCR
366 amplification and ligation into pLV-EF1a-IRES-Blast vector (Addgene, #85133). For DHX9
367 overexpression, wobble mutants were made to reduce shRNA targeting. Mutagenesis primers
368 for DHX9 K417R and shRNA-resistant codons (designed using the Synonymous Mutation

369 Generator⁶⁴) are included in Supplemental Table 1. The DHX9-dsRBD-EGFP construct was
370 generated by digestion of pLV-EF1-DHX9 with SpeI and EcoRI and ligation of EGFP in place of
371 the 3' portion of DHX9. The resulting construct codes for the first 344 amino acids of DHX9
372 fused to EGFP.

373 **Immunoblot**

374 Cell pellets were lysed and sonicated in RIPA Buffer (50 mM Tris pH 7.4 (Ambion), 150
375 mM NaCl (Ambion), 1% Triton X-100 (Sigma-Aldrich), 0.1% sodium dodecyl sulfate (Sigma-
376 Aldrich) and 0.5% sodium deoxycholate (Promega) with 1x HALT Protease Inhibitor (Pierce).
377 Protein was quantified using the DC Assay kit (Bio-Rad) and diluted in SDS Sample Buffer (125
378 mM Tris pH 6.8, 30% glycerol, 10% sodium dodecyl sulfate, 0.012% bromophenol blue) prior to
379 denaturation by heating to 95 °C for 7 minutes. Thirty micrograms of protein lysate were
380 resolved on 4-12% TGX Acrylamide Stain-Free gels (Bio-Rad). Stain-Free gels were imaged
381 prior to transfer to PVDF membrane (Millipore or Bio-Rad) by TransBlot Turbo (Bio-Rad). The
382 blots were then probed with the appropriate primary antibodies: ADAR1 (Santa Cruz, sc-73408;
383 Bethyl Laboratories, A303-883A), DDX17 (Thermo Scientific, PA5-84585), DHX9 (Bethyl, A300-
384 855A), DDX54 (Novus Biologicals, NB100-60678), eIF2a (Abcam, ab5369), eIF2a-Ser-51-P
385 (Abcam, ab32157), Fibrillarin (Santa Cruz, sc-25397), beta-tubulin (Abcam, ab6046), ISG15
386 (Santa Cruz, sc-166755), cleaved PARP (Cell Signaling, #9541), PKR (Cell Signaling, #3072),
387 PKR Thr-446-P (Abcam, ab32036). Primary antibodies were detected with horseradish-
388 peroxidase conjugated secondary antibodies (Jackson ImmunoResearch) and detection was
389 carried out with Clarity Western ECL Substrate (Bio-Rad). Densitometry was performed using
390 Image Lab (Bio-Rad). Band intensity was normalized to total protein measured by imaging of
391 the Stain-Free gel.

392 **Proximity Labeling by APEX2**

393 SK-BR-3, MCF-7, or MDA-MB-231 cells expressing pLVX-puro-FLAG-APEX2 or pLVX-
394 puro-FLAG-APEX2-ADAR1p110 were grown to ~80% confluency in a 15 cm dish. Quencher
395 solution (10 mM sodium azide, 10 mM sodium ascorbate, and 5 mM Trolox (Sigma-Aldrich,
396 238813-1G) in 1X PBS) was prepared at 1X and 2X concentrations. Prior to labeling, cells were
397 incubated in 10 mL of culture media containing 500 μ M biotin phenol (Toronto Research
398 Chemicals, B397770) for 30 min at 37 °C. Next, hydrogen peroxide was added to the cells at 1
399 mM and incubated at room temperature for 1 min. Immediately one volume of 2X quencher
400 solution was added to the cells to stop labeling. The cells were washed twice with 1X quencher
401 solution. Cells were harvested by scraping in 1X quencher solution and lysed in RIPA buffer
402 containing 10 mM sodium azide, 10 mM sodium ascorbate, 5 mM Trolox and 1x HALT. Biotin
403 labeling was verified by immunoblotting with HRP-streptavidin (Abcam, ab7403). Biotinylated
404 proteins were purified using streptavidin magnetic beads (Thermo Fisher Scientific, 88816).
405 Streptavidin magnetic beads were washed twice with RIPA containing HALT and quenching
406 agents. The lysate from above was incubated with the beads for 1 hour at room temperature.
407 The beads were washed in the following order: once with RIPA containing HALT and quenching
408 agents, once with RIPA, once with 1 M KCl, once with 2 M urea pH 8.0, twice in RIPA and once
409 with water. Elution was performed in 1X SDS-Sample buffer by heating at 95 °C for 10 minutes.
410 The eluate was analyzed by LC-MS-MS, see below.

411 **Mass Spectrometry**

412 Liquid-chromatography and tandem mass spectrometry was performed by MSBioWorks
413 (Ann Arbor, MI). The eluates from the streptavidin pulldown above were processed by SDS-
414 PAGE using 10% Bis-Tris NuPage Mini-gel (Invitrogen) with the MES buffer system. The gel
415 was run 2cm. The mobility region was excised and processed by in-gel digestion with trypsin
416 using a robot (ProGest, DigiLab). For the trypsin digestion, the gel slices were washed with
417 25mM ammonium bicarbonate followed by acetonitrile. The samples were reduced with 10mM

418 dithiothreitol at 60°C followed by alkylation with 50mM iodoacetamide at room temperature.
419 Subsequently proteins were digested with trypsin (Promega) at 37°C for 4 h. The trypsin
420 digestion was quenched with formic acid and the supernatant was analyzed directly without
421 further processing. The digested sample was analyzed by nano LC-MS/MS with a Waters M-
422 Class HPLC system interfaced to a ThermoFisher Fusion Lumos mass spectrometer. Peptides
423 were loaded on a trapping column and eluted over a 75 µm analytical column at 350 nL/min;
424 both columns were packed with Luna C18 resin (Phenomenex). The mass spectrometer was
425 operated in data-dependent mode, with the Orbitrap operating at 60,000 FWHM and 15,000
426 FWHM for MS and MS/MS respectively. APD was enabled and the instrument was run with a 3
427 s cycle for MS and MS/MS. Five hours of instrument time was used for the analysis of each
428 sample.

429 **Analysis of Mass Spectrometry Data**

430 Data were searched using a local copy of Mascot (Matrix Science) with the following
431 parameters: Enzyme - Trypsin/P; Database - SwissProt Human (concatenated forward and
432 reverse plus common contaminants); Fixed modification – Carbamidomethyl; Variable
433 modifications - Oxidation; Acetyl; Pyro-Glu; Deamidation; Mass values – Monoisotopic; Peptide
434 Mass Tolerance - 10 ppm; Fragment Mass Tolerance - 0.02 Da; Max Missed Cleavages - 2.
435 Mascot DAT files were parsed into Scaffold (Proteome Software) for validation, filtering and to
436 create a non-redundant list per sample. Data were filtered using a 1% protein and peptide FDR
437 and requiring at least two unique peptides per protein. Fold change of protein abundance was
438 determined by DESeq2 using spectral counts (see Data Availability below for scripts).
439 Overrepresentation analysis was performed using ‘enrichR’ in R⁶⁵. The cutoff used for
440 enrichment for the overrepresentation analysis was an FDR < 0.05 and a log2 fold change of >
441 0.5.

442 **Immunoprecipitation**

443 Cell lysates prepared in RIPA with 1X HALT. RNaseOUT (Thermo Fisher) RNase
444 inhibitor was added to the lysis buffer at 0.5 U/ μ L when RNase A was not used. One milligram
445 of protein lysate was mixed with 2-10 μ g of IgG or specific antibody overnight at 4 °C with
446 rotation. For samples treated with RNase A, 20 μ g of RNase A (Invitrogen) was added to the
447 lysate during overnight mixing with the antibody. Protein G Dynabeads (Thermo Fisher, 25 μ L
448 per sample) were prepared by washing twice in the lysis buffer. Prepared beads were mixed
449 with lysates for 30 min at 4 °C with rotation. Supernatants were collected and beads were
450 washed three times in the lysis buffer, and eluted by mixing the beads in SDS sample buffer and
451 incubating at 95 °C for 7 min. Antibodies: Rabbit IgG (Jackson ImmunoResearch, 011-000-003),
452 Mouse IgG (Jackson ImmunoResearch, 015-000-003), DHX9 (Bethyl, A300-855A), PARP (Cell
453 Signaling, 9532S), XRN2 (Novus, NB100-57541), DDX54 (Novus, NB100-60678), DDX17
454 (Thermo Scientific, PA5-84585).

455 **Immunofluorescence**

456 Cells were plated on glass coverslips (Corning) two days prior to fixation for
457 immunofluorescence. Cells were washed in PBS prior to fixation with 4% paraformaldehyde
458 (Thermo Scientific) and permeabilization with 0.15% Triton-X100 in PBS. Following
459 permeabilization the cells were washed three times with PBS then blocked with Protein Block
460 (Aligent/Dako, X090930-2). Primary antibodies (ADAR1 (Santa Cruz, sc-73408), Fibrillarin
461 (Santa Cruz, sc-25397), DDX54 (Novus Biologicals, NB100-60678) or DDX17 (Thermo
462 Scientific, PA5-84585), DHX9 (Bethyl, A300-855A)) and secondary antibodies (Thermo
463 Scientific, A21207, A21203, A21202, A21206) were diluted in Antibody Diluent (Agilent/Dako,
464 S302283-2). Antibody binding was performed in a humidity chamber for 1.5 hours for primaries
465 and 30 minutes for secondaries. Between primary and secondary antibodies, and after

466 secondary antibody binding the coverslips were washed in PBS. The coverslips were washed
467 once in water before mounting on glass slides with Vectashield Antifade Mounting Media with
468 DAPI (Vector Laboratories, H-1200-10). Fluorescence microscopy images were obtained with
469 an Eclipse 90i microscope (Nikon) using a Plan Apochromatic 20x/NA 0.75 objective (Nikon)
470 and a CoolSNAP ES2 monochrome digital camera cooled to 0°C (Photometrics). Fluorescence
471 images were captured with MetaMorph version 7.8.0.0 software (Molecular Devices) and
472 resized and formatted with Fiji.

473 **Transfection of poly(I:C)**

474 The cell line indicated was transfected with high-molecular weight poly(I:C) (Invivogen)
475 with Lipofectamine LTX. Three microliters of Lipofectamine LTX was used per microgram of
476 poly(I:C). Sixteen hours after transfection, cells were harvested in RIPA with 1X HALT or the
477 RNA lysis buffer from the Nucleospin RNA kit (Macherey-Nagel).

478 **RNA Purification and RNA sequencing**

479 RNA-sequencing was performed for two replicates of ADAR1 and/or DHX9 knockdown
480 in MCF-7 and SK-BR-3. RNA was purified using the Nucleospin RNA kit (Macherey-Nagel).
481 Assessment of rRNA integrity and RNA-sequencing was performed by the Genome Technology
482 Access Center at Washington University in St. Louis. Total RNA integrity was determined using
483 Agilent TapeStation 4200. Library preparation was performed with 500 ng to 1 ug of total RNA.
484 Ribosomal RNA was removed by an RNase-H method using RiboErase kit (Kapa Biosystems).
485 After rRNA depletion, the remaining RNA was then fragmented in reverse transcriptase buffer
486 (Life Technologies) by heating to 94 degrees for 8 minutes. The RNA was reverse transcribed to
487 yield cDNA using SuperScript III RT and random hexamers (Life Technologies) per
488 manufacturer's instructions. A second strand reaction was performed with DNA Polymerase I
489 and RNase H (Qiagen) to yield ds-cDNA. The cDNA was then blunted with T4 DNA

490 Polymerase, Polynucleotide Kinase and Klenow DNA Polymerase (Qiagen). An A base was
491 added to the 3' ends with Klenow (3'-4' exo-) (Qiagen). The processed ds-cDNA was then
492 ligated to Illumina sequencing adapters with T4 DNA Ligase (Qiagen). Ligated fragments were
493 then amplified for 12-15 cycles using primers incorporating unique dual index tags with VeraSeq
494 polymerase (Qiagen). Fragments were sequenced on an Illumina NovaSeq-6000 using paired
495 end reads extending 150 bases.

496 **RNA Sequencing Analysis**

497 The Illumina bcl2fastq software was used for base calling and demultiplexing, allowing
498 for one mismatch in the indexing read. STAR version 2.7.9a1 was used for read alignment to
499 RNA-seq to the Ensembl GRCh38.101 primary assembly. Gene counts were determined using
500 Subread:featureCount version 2.0.32, only uniquely aligned unambiguous reads were counted.
501 Differential gene expression was determined using DESeq2 (see Data Availability below for
502 scripts)⁶⁶. The experimental design for DESeq2 analysis included an interaction term between
503 the shRNAs used for knockdown ('shrna1 + shrna2 + shrna1:shrna2'; where 'shrna1' was either
504 shSCR or shADAR and 'shrna2' was either shSCR or shDHX9-3). Contrasts were used to
505 assess differential expression after singular knockdown of either ADAR1 or DHX9. Fold
506 changes were shrunken using the 'apeglm' approach from DESeq2⁶⁷. Gene set enrichment
507 analysis was performed using 'clusterProfiler'⁶⁸. For analysis of transposable element
508 expression, 'TEcount' from Tetrascripts⁶⁹ was used to determine family level counts for
509 transposable elements using a GTF file containing transposable element information from
510 RepeatMasker (<http://www.repeatmasker.org>). (see Data Availability section for more
511 information about the GTF file).

512 **Foci Formation Assay**

513 Five thousand cells were plated for each condition in a 10 cm culture dish. After 10 (BT-
514 549, MDA-MB-MB231, HCC1806, MDA-MB-468 and SK-BR-3) to 20 (MCF-7) days the cells
515 were washed briefly with 1x PBS prior to fixation in 100% methanol for 5 min. After drying, the
516 cells were stained with 0.005% Crystal Violet solution containing 25% methanol (Sigma-Aldrich)
517 prior to washing excess stain away with deionized water. The plates were scanned using an
518 ImageScanner III (General Electric). Foci area was calculated using ImageJ.

519 **Analysis of CCLE and TCGA data**

520 RNA-seq normalization and calculation of z-scores was performed as described
521 previously³³. Molecular subtypes of breast cancer cell lines and TCGA samples were defined
522 previously⁷⁰. Breast cancer survival analysis was performed using the R packages RTCGA and
523 survminer^{71,72}. The DHX9 expression level used for stratification in survival analysis was
524 determine by the surv_cutpoint function of survminer.

525 **Data and Code Availability**

526 Scripts used for analysis of mass spectrometry, RNA-seq and generation of all plots are
527 available at (<https://github.com/cottrellka/Cottrell-Ryu-et-al-2023>), raw sequencing data and
528 count files were deposited at the Gene Expression Omnibus (GEO) under accession
529 <GSE224677>. RNA-seq data for cancer cell lines (CCLE_expression_full.csv,
530 CCLE_RNAseq_rsem_transcripts_tpm_20180929.txt) were obtained from the DepMap portal
531 (<https://depmap.org/portal/download/custom/>)⁷³. RNAi based dependency data for DHX9
532 (D2_combined_gene_dep_scores) was obtained from DepMap Portal
533 (<https://depmap.org/portal/download/custom/>)⁷⁴. RNA-seq data for TCGA BRCA samples
534 (illuminahisecq_rnaseqv2-RSEM_genes, illuminahisecq_rnaseqv2-RSEM_isoforms_normalized)
535 and clinical data (Merge_Clinical) were obtained from the Broad Institute FireBrowse and are
536 available at <http://firebrowse.org/>. The GTF file used for TEcount

537 (GRCh38_Ensembl_rmsk_TE.gtf) is available at

538 <https://www.dropbox.com/sh/1ppg2e0fbc64bqw/AACUXf-TA1rnBljvykMH2Lcia?dl=0>.

539

540 **Acknowledgements:**

541 The authors would like to thank Leonard B. Maggi, Jr., Raleigh Kladney, Louis Kerestes,
542 Che-Pei Kung, and Anbrielle Blake for technical assistance, Elliot Klotz and Toni Sinnwell
543 (Genome Technology Access Center at Washington University) for RNA sequencing, Joshua B.
544 Rubin, Jason C. Mills, Jieya Shao, and Alessandro Vindigni for discussion and suggestions. The
545 data described here is in part based on data generated by the TCGA Research
546 Network: <https://www.cancer.gov/tcga>. This work was supported by R01CA190986 (J.D.W.),
547 K99MD016946 and R00MD016946 (K.A.C) from the National Institutes of Health, W81XWH-18-
548 1-0025 (J.D.W.) and W81XWH-21-10466 (J.D.W.) from the Department of Defense, and a
549 Centene Corporation Contract (P19-00559) for the Washington University–Centene ARCH
550 Personalized Medicine Initiative (J.D.W.). L.S.T. supported by R25HG006687 and
551 T32GM148405.

552

553 **Author Contributions**

554 K.A.C, S.R. and J.D.W. conceived the project. K.A.C., S.R., L.S.T., and A.M.S.
555 performed the experiments. K.A.C., S.R., and L.S.T. performed the data analysis. K.A.C. and
556 S.R. wrote the manuscript. All authors edited the manuscript.

557

558 **Figure 1: Identification of putative ADAR1 interacting proteins by APEX2 proximity**
559 **labeling**

560 **a** Immunoblot showing expression of the constructs used for proximity labeling in MCF-7, MDA-
561 MB-231 and SK-BR-3. **b** Representative fluorescently stained gel image showing proteins
562 purified by streptavidin-biotin pulldown following proximity labeling in MCF-7. **c** Volcano plot
563 summarizing the proteins identified by mass spectrometry following streptavidin pulldown
564 subsequent to proximity labeling. Differential abundance of all proteins in each cell line can be
565 found in Supplementary Table 2. **d** Venn diagram showing overlap between enriched proteins
566 from all three cell lines. The cut-off for enriched proteins was an FDR adjusted p-value of less
567 than 0.05 and a Log₂ fold change of greater than 0.5. **e** GO terms found to be overrepresented
568 in the list of the enriched proteins. Only the top ten GO terms, by FDR, are shown for each
569 category. All other significant GO terms are available in the Supplementary Table 3-4. **f** and **g**
570 Venn diagrams showing overlap between the enriched proteins identified and those proteins
571 found previously to localize to the nucleus or nucleolus in MCF-7⁴³. **h** Representative indirect
572 immunofluorescence micrographs showing localization of ADAR1, fibrillarin (a nucleolar marker)
573 and DAPI.

574 **Figure 2: Validation of putative protein-protein interactions identified by proximity**
575 **labeling**

576 Immunoprecipitation of DHX9 **a-c**, DDX54 **d-e** or DDX17 **f-g** followed by immunoblot for ADAR
577 in breast cancer cell lines. Immunoblot of immunoprecipitation eluates and inputs from SK-BR-3
578 **a, d and f**, MCF-7 **b, e and g**, and MDA-MB-231 **c**. Input represents 5% of the lysate used for
579 immunoprecipitation. The IgG lanes represent immunoprecipitation eluates from pulldown with
580 anti-rabbit IgG antibody. The lanes labeled DHX9, DDX54 and DDX17 indicate the eluates from
581 immunoprecipitation with antibodies against those proteins respectively. The IgG^{HC} label
582 indicates the band corresponding to the IgG heavy chain from the antibody used for
583 immunoprecipitation. Uncropped immunoblots for panels **a-g** can be found in Source Data
584 Figures. Immunofluorescence for ADAR1 and DHX9 **h**, DDX54 **i**, or DDX17 **j** in SKBR3 or MCF-
585 7.
586

587 **Figure 3: DHX9 is overexpressed in breast cancer and suppresses PKR activation**

588 **a** Schematic showing the domain structure of PKR, ADAR1, DHX9 and other helicases
589 identified by proximity labeling in Fig. 1, dsRBD refers to the dsRNA Binding Domain. **b**
590 Pearson and Spearman correlation coefficients for the correlation between ADAR1 expression
591 at the RNA level and the expression of each indicated helicase at the RNA level, data from
592 breast tumors within TCGA. Scatterplots showing the correlation between ADAR1-p110 **c**, or
593 ADAR1-p150 **d**, and DHX9 expression in normal breast or breast tumors. **e** Expression of DHX9
594 at the RNA level in normal breast, non-TNBC or TNBC tumors. **f** Waterfall plot showing DHX9
595 dependency of breast cancer cell lines using data from DepMap, ER = estrogen receptor
596 positive cell lines, ERB2 = HER2 positive cell lines. **g** Representative immunoblot following
597 knockdown of DHX9 with two different shRNAs in four TNBC cell lines. Immunoblots for other
598 replicates and uncropped blots can be found in Source Data Figures. **h** Foci formation assay for
599 the same cells used in **g** for immunoblot. **i** Quantification of PKR phosphorylation as determined
600 by the immunoblot in **g**. Quantification of protein expression for other proteins of interest can be
601 found in Extended Data Fig. 3a-e. Bars represent the average of at least three replicates, error
602 bars are +/- SD. * p <0.05, ** p <0.01, *** p < 0.001. P-values determined by Dunnett's test.
603

604 **Figure 4: DHX9 and ADAR1 redundantly suppress dsRNA sensing in ADAR1-independent**
605 **cell lines**

606 Representative immunoblot showing the phenotype of ADAR1 and/or DHX9 knockdown in
607 MCF-7 **a**, or SK-BR-3 **f**. Immunoblots for other replicates and uncropped blots can be found in
608 Source Data Figures. Protein abundance from the immunoblot in **a** and **f** was normalized by
609 total protein abundance by quantification of the Stain Free gel in **b** and **g** respectively. Fold
610 change of PKR phosphorylation at Thr-446 in MCF-7 **d** or SK-BR-3 **i** as determined by the
611 immunoblots in **a** or **f** respectively. Quantification of protein expression for other proteins of
612 interest can be found in Extended Data Fig. 4a-l. Representative foci formation phenotype of
613 ADAR1 and/or DHX9 knockdown in MCF-7 **c** or SK-BR-3 **h**, quantification of relative foci area is
614 shown in **e** or **j** respectively. **k** Analysis of rRNA integrity upon knockdown of ADAR1 and/or
615 DHX9 in MCF-7 or SK-BR-3. Additionally, panel **k** shows the effect of poly(I:C) (p(I:C))
616 transfection on rRNA integrity in MCF-7. Bars represent the average of at least three replicates,
617 error bars are +/- SD. * $p < 0.05$, ** $p < 0.01$, *** $p < 0.001$. P-values determined by one-way
618 ANOVA with post-hoc Tukey. Comparisons between the two different shRNAs targeting DHX9
619 (shDHX9-3 and shDHX9-5) were not included for clarity.
620

621 **Figure 5: Induction of a viral mimicry phenotype upon knockdown of DHX9 and ADAR1 in**
622 **MCF-7**

623 **A** Volcano plot showing changes in RNA expression upon knockdown of DHX9 and ADAR1 in
624 MCF-7, a volcano plot for SK-BR-3 is in Extended Data Fig. 5f. Fold-change of RNA expression
625 shown in **a** was determined using an interaction term between ADAR1 and DHX9 knockdown,
626 volcano plots for fold change of RNA expression for single knockdown of ADAR1 or DHX9 is in
627 Extended Data Fig. 5a-b and 5d-e. **b** GO terms identified by gene set enrichment analysis of the
628 RNA-seq data in **a**. **c-e** Heatmaps and summary box plots showing RNA expression changes in
629 MCF-7 and SK-BR-3 upon knockdown of ADAR1 and/or DHX9. Panel **c** shows RNA expression
630 for core ISGs^{21,33}, panel **d** shows ATF4 targets and panel **e** shows NF-KB targets with ISGs
631 removed.

632 **Figure 6: Rescue of PKR activation by ADAR1-p110, ADAR-p150, DHX9 and DHX9**
633 **mutants**

634 **a** Schematic showing the domain structure of ADAR1 isoforms, DHX9 and mutants of DHX9,
635 dsRBD refers to the dsRNA Binding Domain. Representative immunoblot showing the
636 phenotype of ADAR1 and DHX9 knockdown with DHX9, DHX9^{K417R} or dsRBD-EGFP
637 overexpression **b**, or ADAR1 isoform overexpression **f**. Immunoblots for other replicates and
638 uncropped blots can be found in Source Data Figures. Fold change of PKR phosphorylation at
639 Thr-446 upon ADAR1 and DHX9 knockdown with DHX9, DHX9^{K417R} or dsRBD-EGFP
640 overexpression **d**, or ADAR1 isoform overexpression **h**, quantified from immunoblots in **b** and **f**
641 respectively. Quantification of protein expression for other proteins of interest can be found in
642 Extended Data Fig. 7b-f and 8a-f. Representative foci formation phenotype of ADAR1 and
643 DHX9 knockdown with DHX9, DHX9^{K417R} or dsRBD-EGFP overexpression **c**, or ADAR1 isoform
644 overexpression **g**. Quantification of relative foci area is shown in **e** or **i**, respectively. Bars
645 represent the average of at least three replicates, error bars are +/- SD. * p < 0.05, ** p < 0.01,
646 *** p < 0.001. P-values determined by Dunnett's test.

647

648 **Figure 7: Model of ADAR1 and DHX9s roles in suppression of dsRNA sensing.**

649 A hypothetical model based on published data and the findings presented here. Dashed lines
650 indicate multiple steps. Lines marked with question marks are proposed and require further
651 investigation. Created with BioRender.com
652

653 **References**

- 654 1. Paz-Yaacov, N. *et al.* Elevated RNA Editing Activity Is a Major Contributor to Transcriptomic
655 Diversity in Tumors. *Cell Rep.* **13**, 267–276 (2015).
- 656 2. Walkley, C. R. & Li, J. B. Rewriting the transcriptome: adenosine-to-inosine RNA editing by
657 ADARs. *Genome Biol.* **18**, 205 (2017).
- 658 3. Li, M. *et al.* Widespread RNA and DNA Sequence Differences in the Human Transcriptome.
659 *Science* **333**, 53–58 (2011).
- 660 4. Bazak, L. *et al.* A-to-I RNA editing occurs at over a hundred million genomic sites, located in
661 a majority of human genes. *Genome Res.* **24**, 365–376 (2014).
- 662 5. Wagner, R. W., Smith, J. E., Cooperman, B. S. & Nishikura, K. A double-stranded RNA
663 unwinding activity introduces structural alterations by means of adenosine to inosine
664 conversions in mammalian cells and *Xenopus* eggs. *Proc. Natl. Acad. Sci.* **86**, 2647–2651
665 (1989).
- 666 6. Kim, U., Wang, Y., Sanford, T., Zeng, Y. & Nishikura, K. Molecular cloning of cDNA for
667 double-stranded RNA adenosine deaminase, a candidate enzyme for nuclear RNA editing.
668 *Proc. Natl. Acad. Sci.* **91**, 11457–11461 (1994).
- 669 7. Herbert, A. *et al.* A Z-DNA binding domain present in the human editing enzyme, double-
670 stranded RNA adenosine deaminase. *Proc. Natl. Acad. Sci.* **94**, 8421–8426 (1997).
- 671 8. George, C. X. & Samuel, C. E. Human RNA-specific adenosine deaminase ADAR1
672 transcripts possess alternative exon 1 structures that initiate from different promoters, one
673 constitutively active and the other interferon inducible. *Proc. Natl. Acad. Sci.* **96**, 4621–4626
674 (1999).
- 675 9. Desterro, J. M. P. *et al.* Dynamic association of RNA-editing enzymes with the nucleolus. *J.*
676 *Cell Sci.* **116**, 1805–1818 (2003).

- 677 10. Patterson, J. B. & Samuel, C. E. Expression and regulation by interferon of a double-
678 stranded-RNA-specific adenosine deaminase from human cells: evidence for two forms of
679 the deaminase. *Mol. Cell. Biol.* **15**, 5376–5388 (1995).
- 680 11. Eckmann, C. R., Neunteufl, A., Pfaffstetter, L. & Jantsch, M. F. The human but not the
681 *Xenopus* RNA-editing enzyme ADAR1 has an atypical nuclear localization signal and
682 displays the characteristics of a shuttling protein. *Mol. Biol. Cell* **12**, 1911–1924 (2001).
- 683 12. Chung, H. *et al.* Human ADAR1 Prevents Endogenous RNA from Triggering Translational
684 Shutdown. *Cell* **172**, 811-824.e14 (2018).
- 685 13. Liddicoat, B. J. *et al.* RNA editing by ADAR1 prevents MDA5 sensing of endogenous dsRNA
686 as nonself. *Science* **349**, 1115–1120 (2015).
- 687 14. Pestal, K. *et al.* Isoforms of the RNA editing enzyme ADAR1 independently control nucleic
688 acid sensor MDA5-driven autoimmunity and multi-organ development. *Immunity* **43**, 933–
689 944 (2015).
- 690 15. Mannion, N. M. *et al.* The RNA-Editing Enzyme ADAR1 Controls Innate Immune Responses
691 to RNA. *Cell Rep.* **9**, 1482–1494 (2014).
- 692 16. Chen, Y. G. & Hur, S. Cellular origins of dsRNA, their recognition and consequences. *Nat.*
693 *Rev. Mol. Cell Biol.* **23**, 286–301 (2022).
- 694 17. Yang, S. *et al.* ADAR1 Limits RIG-I RNA Detection and Suppresses IFN Production
695 Responding to Viral and Endogenous RNAs. *J. Immunol. Baltim. Md 1950* **193**, 3436–3445
696 (2014).
- 697 18. Clerzius, G. *et al.* ADAR1 Interacts with PKR during Human Immunodeficiency Virus
698 Infection of Lymphocytes and Contributes to Viral Replication. *J. Virol.* **83**, 10119–10128
699 (2009).
- 700 19. Quin, J. *et al.* ADAR RNA Modifications, the Epitranscriptome and Innate Immunity. *Trends*
701 *Biochem. Sci.* **46**, 758–771 (2021).

- 702 20. Montavon, T. C. *et al.* Human DICER helicase domain recruits PKR and modulates its
703 antiviral activity. *PLoS Pathog.* **17**, e1009549 (2021).
- 704 21. Liu, H. *et al.* Tumor-derived IFN triggers chronic pathway agonism and sensitivity to ADAR
705 loss. *Nat. Med.* **25**, 95–102 (2019).
- 706 22. Li, Y. *et al.* Ribonuclease L mediates the cell-lethal phenotype of double-stranded RNA
707 editing enzyme ADAR1 deficiency in a human cell line. *eLife* **6**, e25687 (2017).
- 708 23. Rath, S. *et al.* Concerted 2-5A-Mediated mRNA Decay and Transcription Reprogram
709 Protein Synthesis in the dsRNA Response. *Mol. Cell* **75**, 1218-1228.e6 (2019).
- 710 24. Schoggins, J. W. & Rice, C. M. Interferon-stimulated genes and their antiviral effector
711 functions. *Curr. Opin. Virol.* **1**, 519–525 (2011).
- 712 25. George, C. X., Das, S. & Samuel, C. E. Organization of the mouse RNA-specific adenosine
713 deaminase Adar1 gene 5'-region and demonstration of STAT1-independent, STAT2-
714 dependent transcriptional activation by interferon. *Virology* **380**, 338–343 (2008).
- 715 26. Sun, T. *et al.* Decoupling expression and editing preferences of ADAR1 p150 and p110
716 isoforms. *Proc. Natl. Acad. Sci.* **118**, e2021757118 (2021).
- 717 27. Shiromoto, Y., Sakurai, M., Minakuchi, M., Ariyoshi, K. & Nishikura, K. ADAR1 RNA editing
718 enzyme regulates R-loop formation and genome stability at telomeres in cancer cells. *Nat.*
719 *Commun.* **12**, 1654 (2021).
- 720 28. Fumagalli, D. *et al.* Principles Governing A-to-I RNA Editing in the Breast Cancer
721 Transcriptome. *Cell Rep.* **13**, 277–289 (2015).
- 722 29. Kung, C.-P., Maggi, L. B. & Weber, J. D. The Role of RNA Editing in Cancer Development
723 and Metabolic Disorders. *Front. Endocrinol.* **9**, (2018).
- 724 30. Paz, N. *et al.* Altered adenosine-to-inosine RNA editing in human cancer. *Genome Res.* **17**,
725 1586–1595 (2007).
- 726 31. Chan, T. H. M. *et al.* A disrupted RNA editing balance mediated by ADARs (Adenosine
727 DeAminases that act on RNA) in human hepatocellular carcinoma. *Gut* **63**, 832–843 (2014).

- 728 32. Gannon, H. S. *et al.* Identification of ADAR1 adenosine deaminase dependency in a subset
729 of cancer cells. *Nat. Commun.* **9**, 5450 (2018).
- 730 33. Kung, C.-P. *et al.* Evaluating the therapeutic potential of ADAR1 inhibition for triple-negative
731 breast cancer. *Oncogene* **40**, 189–202 (2021).
- 732 34. Ota, H. *et al.* ADAR1 forms a complex with Dicer to promote microRNA processing and
733 RNA-induced gene silencing. *Cell* **153**, 575–589 (2013).
- 734 35. Freund, E. C. *et al.* Unbiased Identification of trans Regulators of ADAR and A-to-I RNA
735 Editing. *Cell Rep.* **31**, 107656 (2020).
- 736 36. Sakurai, M. *et al.* ADAR1 controls apoptosis of stressed cells by inhibiting Staufen1-
737 mediated mRNA decay. *Nat. Struct. Mol. Biol.* **24**, 534–543 (2017).
- 738 37. Jimeno, S. *et al.* ADAR-mediated RNA editing of DNA:RNA hybrids is required for DNA
739 double strand break repair. *Nat. Commun.* **12**, 5512 (2021).
- 740 38. Hong, H. *et al.* Bidirectional regulation of adenosine-to-inosine (A-to-I) RNA editing by
741 DEAH box helicase 9 (DHX9) in cancer. *Nucleic Acids Res.* **46**, 7953–7969 (2018).
- 742 39. Rajendren, S. *et al.* A protein–protein interaction underlies the molecular basis for substrate
743 recognition by an adenosine-to-inosine RNA-editing enzyme. *Nucleic Acids Res.* **46**, 9647–
744 9659 (2018).
- 745 40. Sapiro, A. L. *et al.* Zinc Finger RNA-Binding Protein Zn72D Regulates ADAR-Mediated RNA
746 Editing in Neurons. *Cell Rep.* **31**, 107654 (2020).
- 747 41. Shamay-Ramot, A. *et al.* Fmrp Interacts with Adar and Regulates RNA Editing, Synaptic
748 Density and Locomotor Activity in Zebrafish. *PLOS Genet.* **11**, e1005702 (2015).
- 749 42. Lam, S. S. *et al.* Directed evolution of APEX2 for electron microscopy and proximity
750 labeling. *Nat. Methods* **12**, 51–54 (2015).
- 751 43. Orre, L. M. *et al.* SubCellBarCode: Proteome-wide Mapping of Protein Localization and
752 Relocalization. *Mol. Cell* **73**, 166-182.e7 (2019).

- 753 44. Aktaş, T. *et al.* DHX9 suppresses RNA processing defects originating from the Alu invasion
754 of the human genome. *Nature* **544**, 115–119 (2017).
- 755 45. Iordanov, M. S. *et al.* Activation of p38 mitogen-activated protein kinase and c-Jun NH(2)-
756 terminal kinase by double-stranded RNA and encephalomyocarditis virus: involvement of
757 RNase L, protein kinase R, and alternative pathways. *Mol. Cell. Biol.* **20**, 617–627 (2000).
- 758 46. Burke, J. M., Gilchrist, A. R., Sawyer, S. L. & Parker, R. RNase L limits host and viral protein
759 synthesis via inhibition of mRNA export. *Sci. Adv.* **7**, eabh2479 (2021).
- 760 47. Nakajima, T. *et al.* RNA helicase A mediates association of CBP with RNA polymerase II.
761 *Cell* **90**, 1107–1112 (1997).
- 762 48. Sadler, A. J., Latchoumanin, O., Hawkes, D., Mak, J. & Williams, B. R. G. An Antiviral
763 Response Directed by PKR Phosphorylation of the RNA Helicase A. *PLOS Pathog.* **5**,
764 e1000311 (2009).
- 765 49. Fuchsová, B. & Hozák, P. The Localization of Nuclear DNA Helicase II in Different Nuclear
766 Compartments Is Linked to Transcription. *Exp. Cell Res.* **279**, 260–270 (2002).
- 767 50. Jeffrey, I. W. *et al.* Nuclear localization of the interferon-inducible protein kinase PKR in
768 human cells and transfected mouse cells. *Exp. Cell Res.* **218**, 17–27 (1995).
- 769 51. García, M. A. *et al.* Impact of protein kinase PKR in cell biology: from antiviral to
770 antiproliferative action. *Microbiol. Mol. Biol. Rev. MMBR* **70**, 1032–1060 (2006).
- 771 52. Lee, T. & Pelletier, J. The biology of DHX9 and its potential as a therapeutic target.
772 *Oncotarget* **7**, 42716–42739 (2016).
- 773 53. ADAR1p150 Prevents MDA5 and PKR Activation via Distinct Mechanisms to Avert Fatal
774 Autoinflammation | bioRxiv. <https://www.biorxiv.org/content/10.1101/2023.01.25.525475v1>.
- 775 54. Harding, H. P. *et al.* Regulated Translation Initiation Controls Stress-Induced Gene
776 Expression in Mammalian Cells. *Mol. Cell* **6**, 1099–1108 (2000).
- 777 55. Pakos-Zebrucka, K. *et al.* The integrated stress response. *EMBO Rep.* **17**, 1374–1395
778 (2016).

- 779 56. Zamanian-Daryoush, M., Mogensen, T. H., DiDonato, J. A. & Williams, B. R. G. NF- κ B
780 Activation by Double-Stranded-RNA-Activated Protein Kinase (PKR) Is Mediated through
781 NF- κ B-Inducing Kinase and I κ B Kinase. *Mol. Cell. Biol.* **20**, 1278–1290 (2000).
- 782 57. Roulois, D. *et al.* DNA-Demethylating Agents Target Colorectal Cancer Cells by Inducing
783 Viral Mimicry by Endogenous Transcripts. *Cell* **162**, 961–973 (2015).
- 784 58. Chen, R., Ishak, C. A. & De Carvalho, D. D. Endogenous Retroelements and the Viral
785 Mimicry Response in Cancer Therapy and Cellular Homeostasis. *Cancer Discov.* **11**, 2707–
786 2725 (2021).
- 787 59. Jansz, N. & Faulkner, G. J. Endogenous retroviruses in the origins and treatment of cancer.
788 *Genome Biol.* **22**, 147 (2021).
- 789 60. Wu, Q. *et al.* PRMT inhibition induces a viral mimicry response in triple-negative breast
790 cancer. *Nat. Chem. Biol.* **18**, 821–830 (2022).
- 791 61. Zhou, X. *et al.* Pharmacologic Activation of p53 Triggers Viral Mimicry Response Thereby
792 Abolishing Tumor Immune Evasion and Promoting Antitumor Immunity. *Cancer Discov.* **11**,
793 3090–3105 (2021).
- 794 62. Sheng, W. *et al.* LSD1 Ablation Stimulates Anti-tumor Immunity and Enables Checkpoint
795 Blockade. *Cell* **174**, 549-563.e19 (2018).
- 796 63. Goel, S. *et al.* CDK4/6 inhibition triggers anti-tumour immunity. *Nature* **548**, 471–475 (2017).
- 797 64. Ong, J. Y. Synonymous Mutation Generator: a web tool for designing RNAi-resistant
798 sequences. 2021.01.02.425100 Preprint at <https://doi.org/10.1101/2021.01.02.425100>
799 (2021).
- 800 65. Kuleshov, M. V. *et al.* Enrichr: a comprehensive gene set enrichment analysis web server
801 2016 update. *Nucleic Acids Res.* **44**, W90–W97 (2016).
- 802 66. Love, M. I., Huber, W. & Anders, S. Moderated estimation of fold change and dispersion for
803 RNA-seq data with DESeq2. *Genome Biol.* **15**, 550 (2014).

- 804 67. Zhu, A., Ibrahim, J. G. & Love, M. I. Heavy-tailed prior distributions for sequence count data:
805 removing the noise and preserving large differences. *Bioinforma. Oxf. Engl.* **35**, 2084–2092
806 (2019).
- 807 68. Wu, T. *et al.* clusterProfiler 4.0: A universal enrichment tool for interpreting omics data.
808 *Innov. Camb. Mass* **2**, 100141 (2021).
- 809 69. Jin, Y., Tam, O. H., Paniagua, E. & Hammell, M. Tetranscripts: a package for including
810 transposable elements in differential expression analysis of RNA-seq datasets. *Bioinforma.*
811 *Oxf. Engl.* **31**, 3593–3599 (2015).
- 812 70. Marcotte, R. *et al.* Functional Genomic Landscape of Human Breast Cancer Drivers,
813 Vulnerabilities, and Resistance. *Cell* **164**, 293–309 (2016).
- 814 71. Kosinski, M., Biecek, P. & Chodor, W. RTCGA: The Cancer Genome Atlas Data Integration.
815 (2022) doi:10.18129/B9.bioc.RTCGA.
- 816 72. Kassambara, A., Kosinski, M., Biecek, P. & Fabian, S. survminer: Drawing Survival Curves
817 using 'ggplot2'. (2020).
- 818 73. Ghandi, M. *et al.* Next-generation characterization of the Cancer Cell Line Encyclopedia.
819 *Nature* **569**, 503–508 (2019).
- 820 74. DepMap 22Q4 Public. (2022) doi:10.6084/m9.figshare.21637199.v2.
- 821

Figure 1

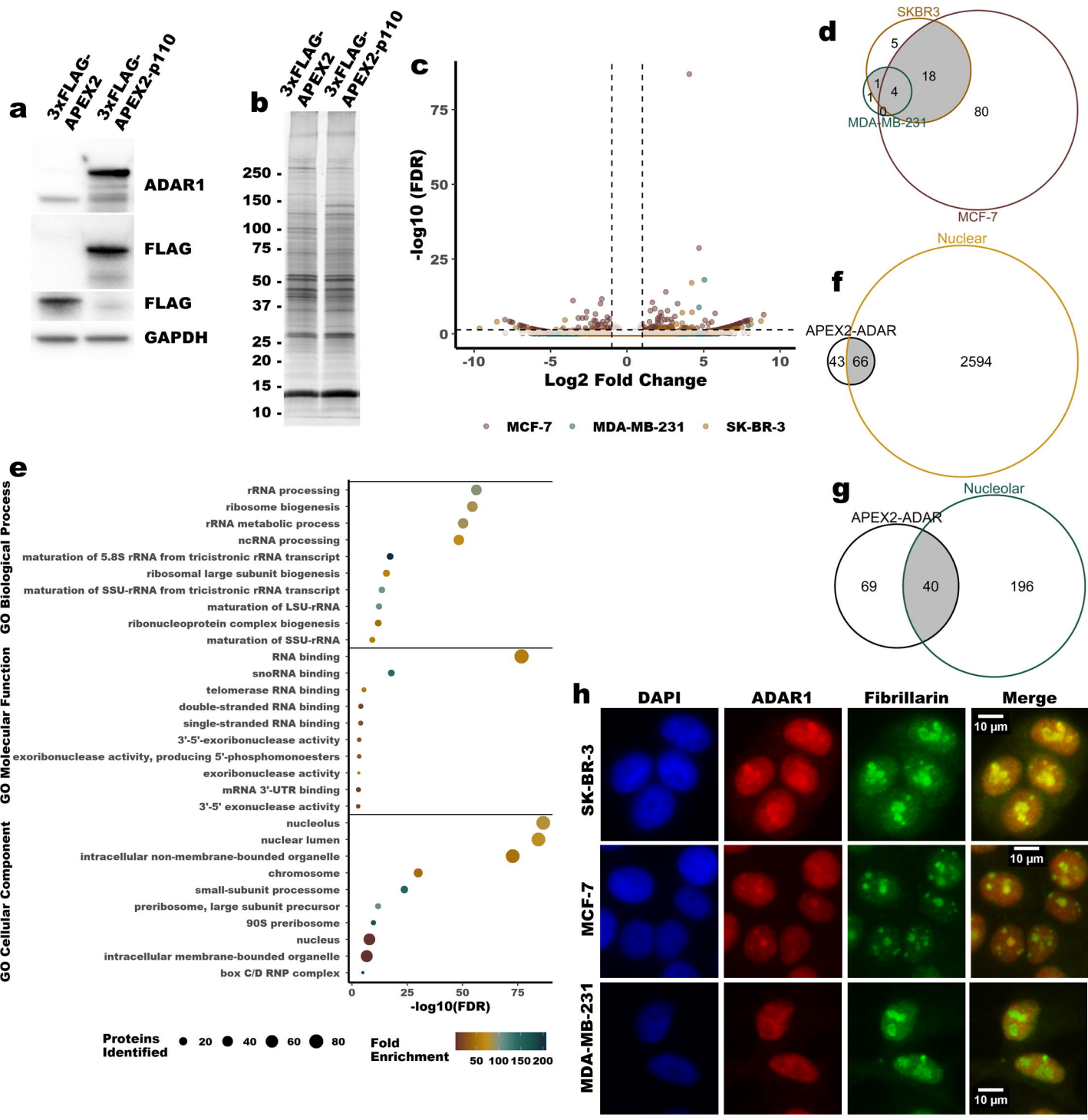


Figure 2

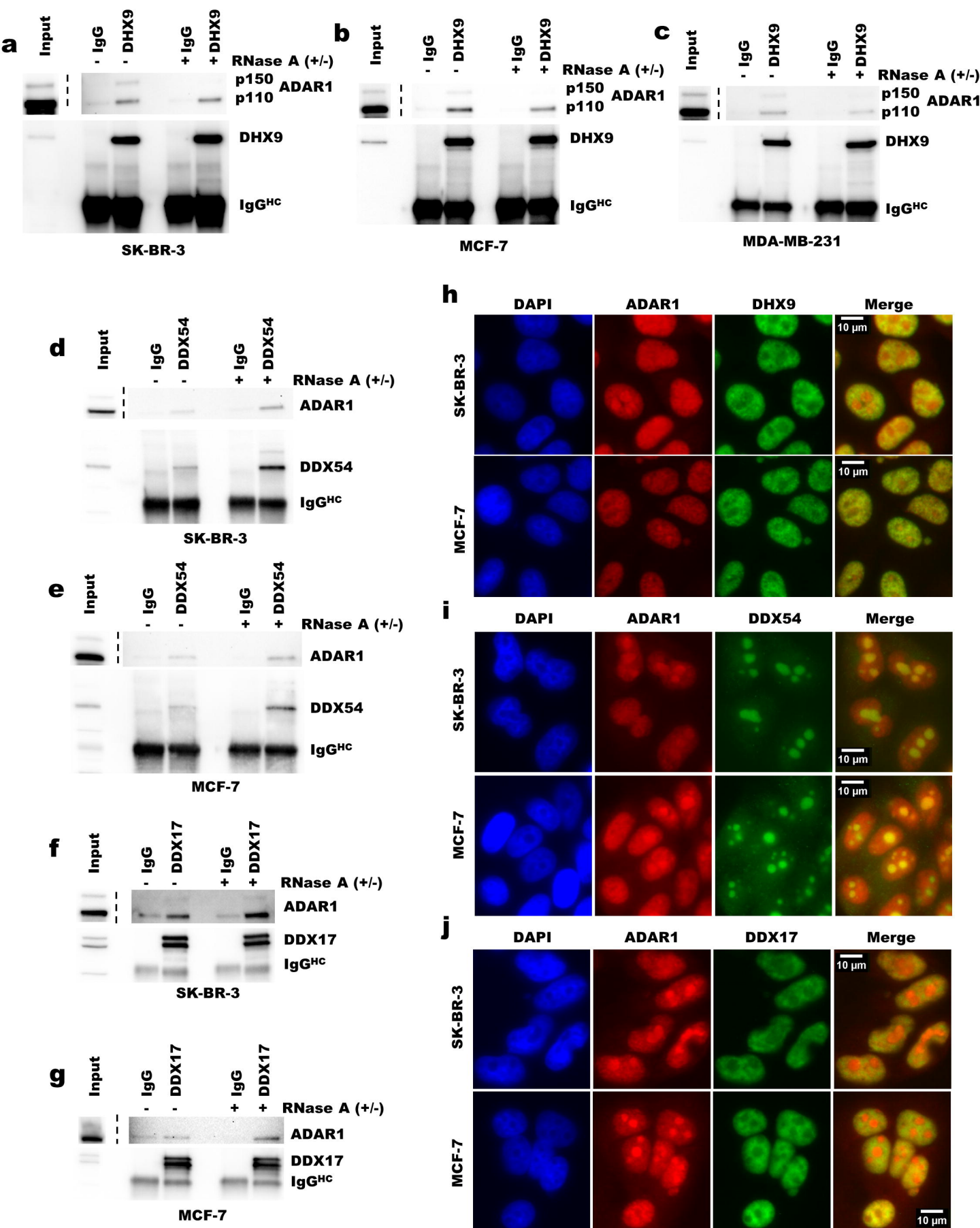


Figure 3

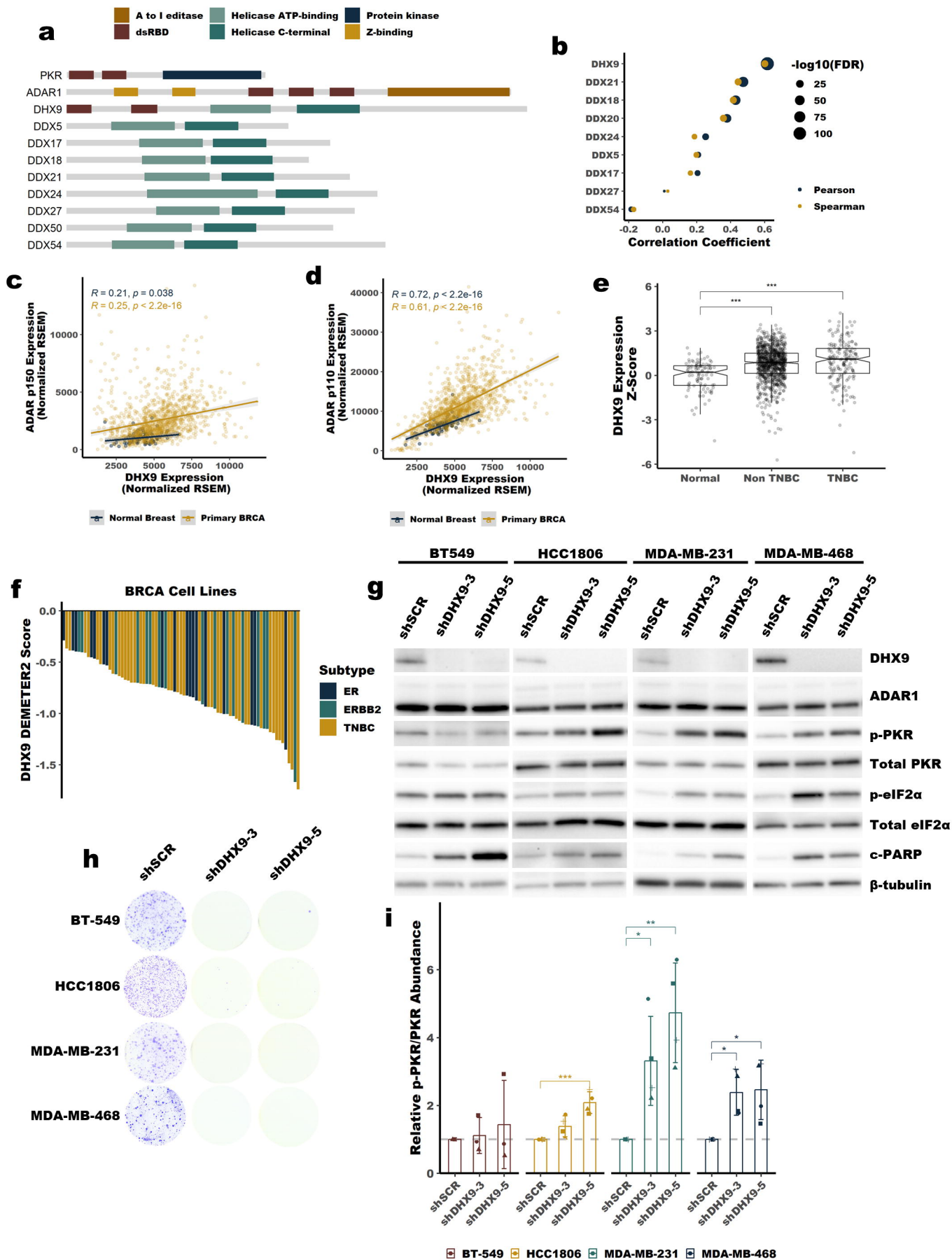
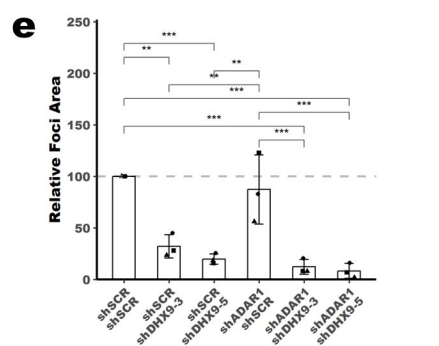
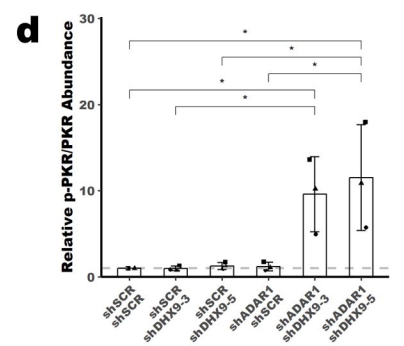
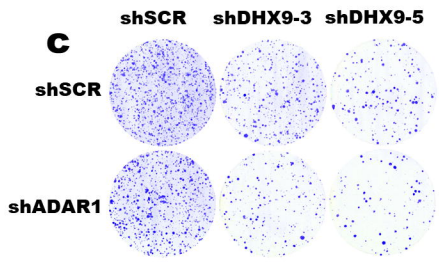
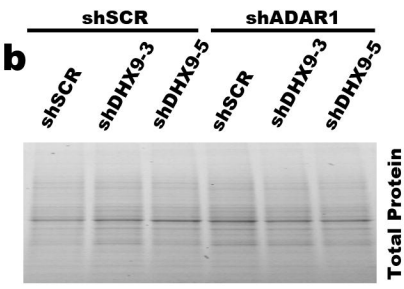
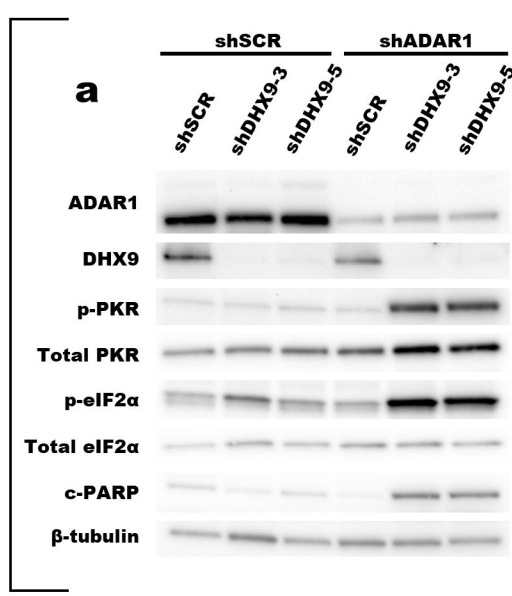


Figure 4

MCF-7



SK-BR-3

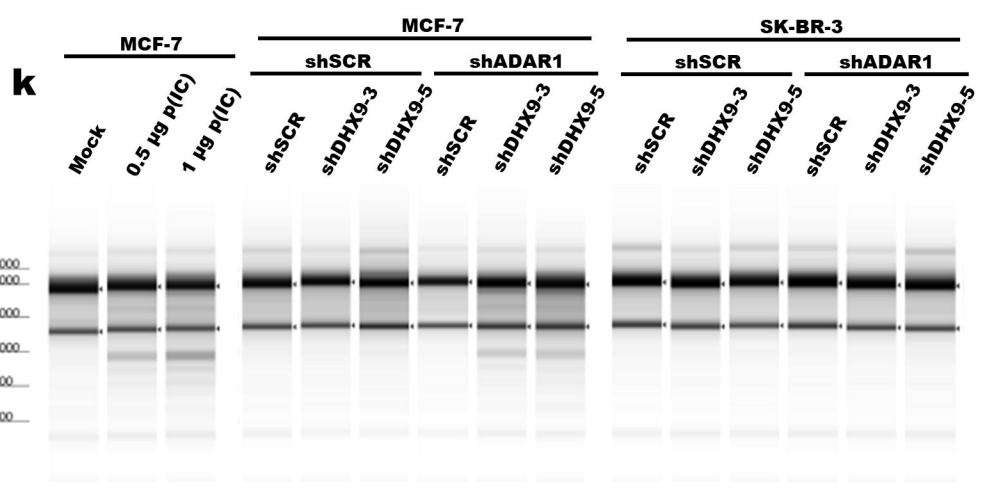
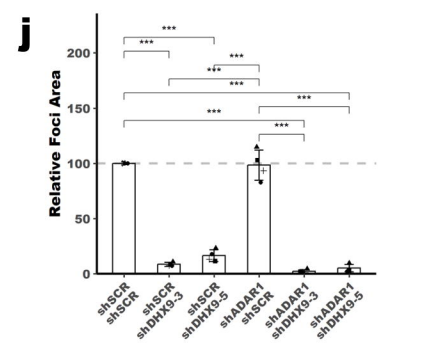
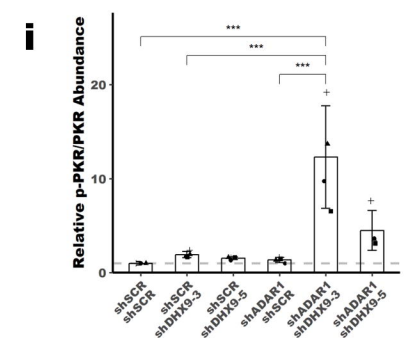
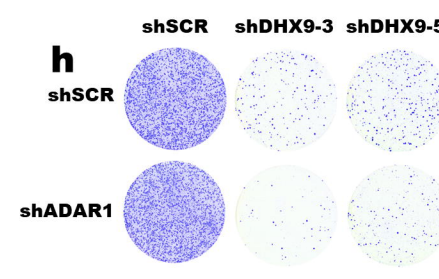
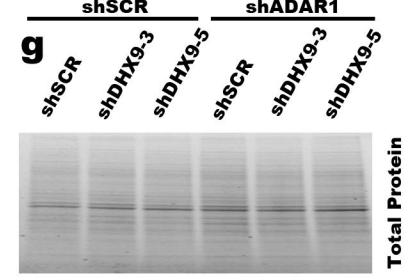
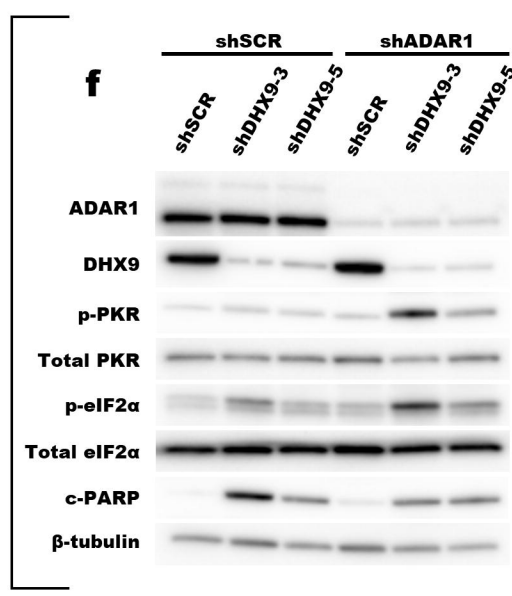


Figure 5

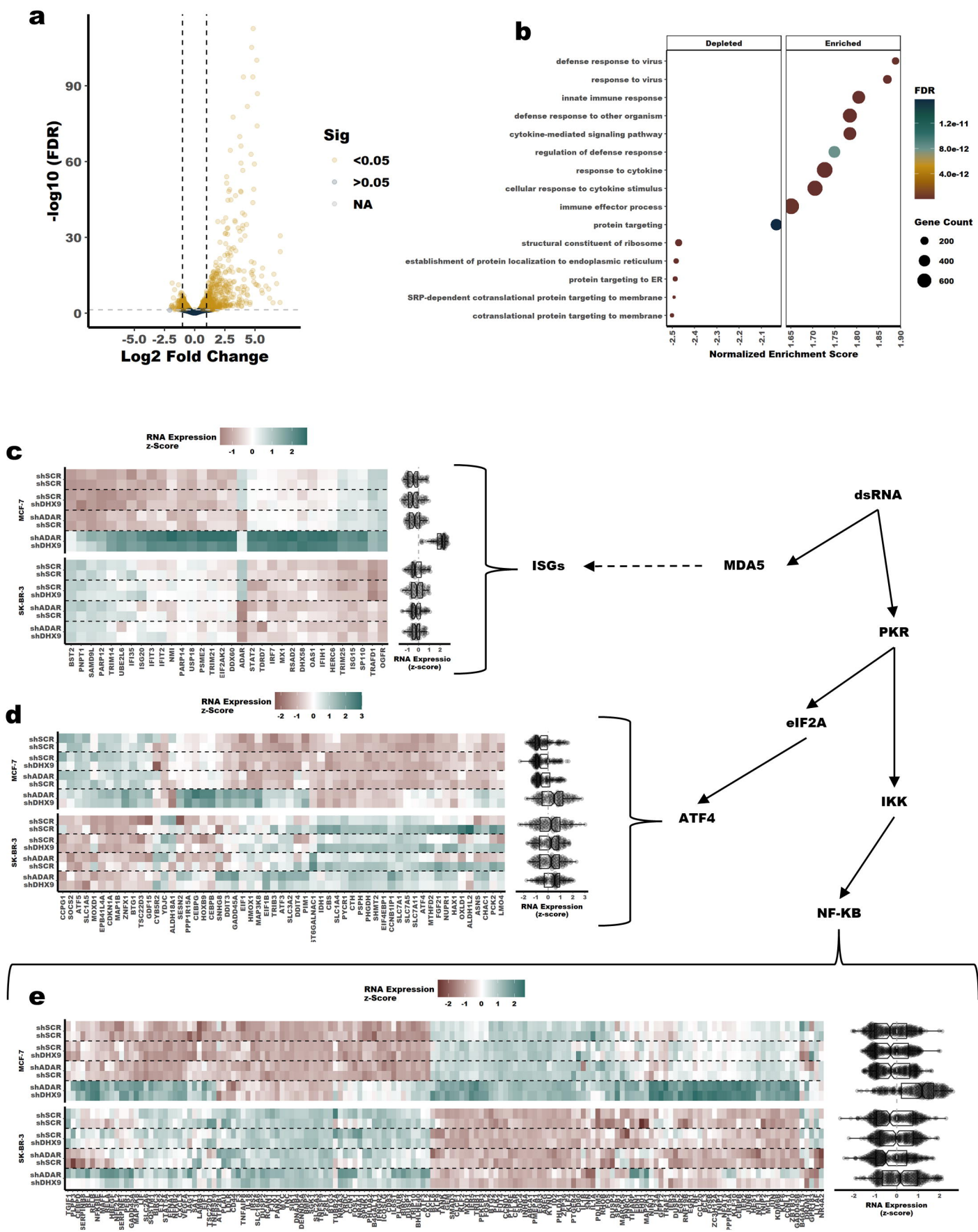


Figure 6

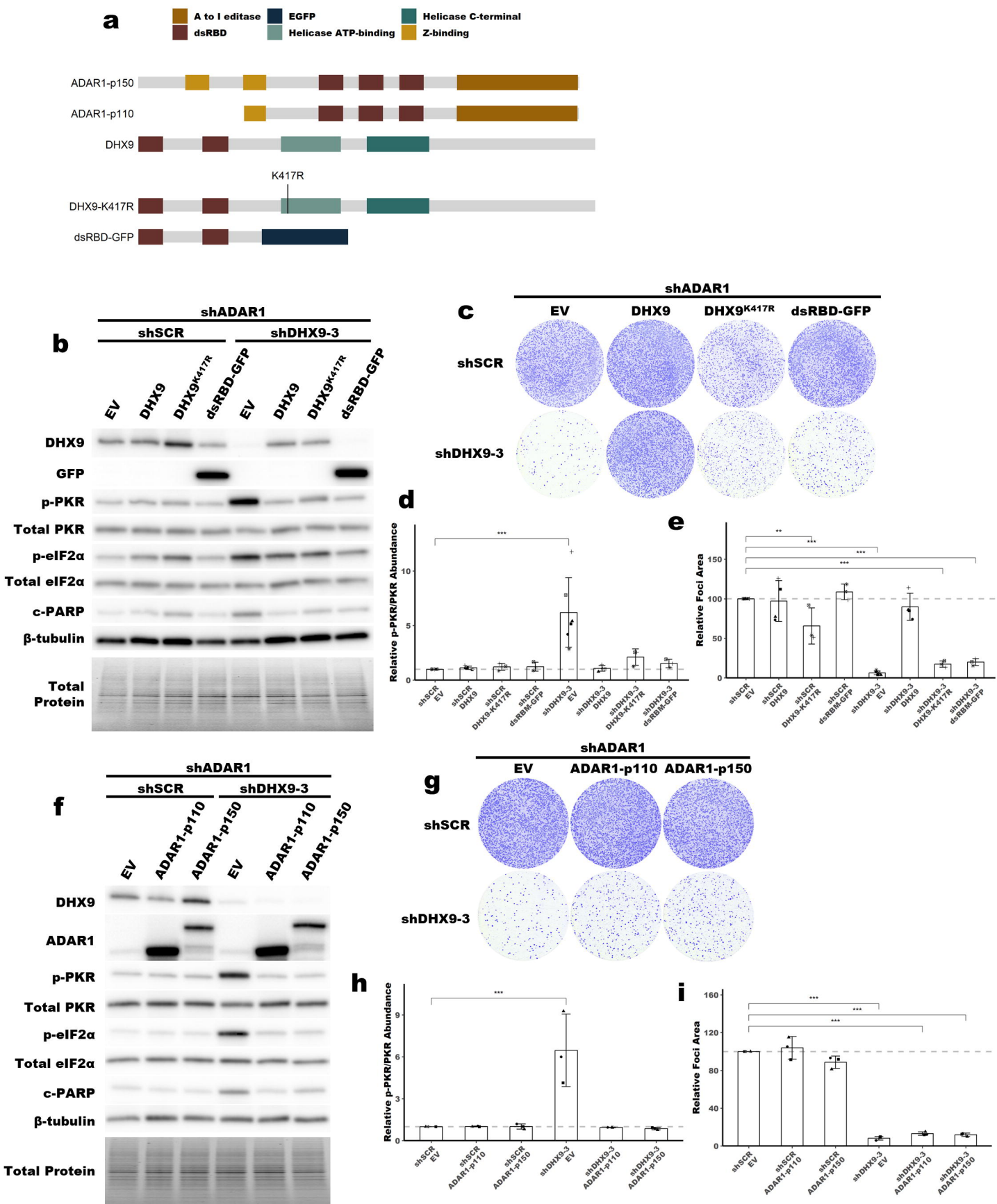


Figure 7

